Tunnel-piled structure interaction: numerical simulation of hybrid centrifuge tests

Geyang Song[a,*], Alec M. Marshall[b]

[a] *Department of Engineering Science, University of Oxford, Parks Road, Oxford, OX1 3PJ, United Kingdom. Formally Faculty of Engineering, University of Nottingham, University Park, NG7 2RD Nottingham, United Kingdom.*
[b] *Faculty of Engineering, University of Nottingham, University Park, NG7 2RD Nottingham, United Kingdom.*

Abstract

Tunnel excavation in urban areas causes ground movements that could damage existing nearby piled structures. Geotechnical centrifuge modelling has been widely used as a tool to study problems related to tunnelling activities and its interaction with existing infrastructure systems. Recent hybrid centrifuge tests using the Coupled Centrifuge-Numerical Modelling (CCNM) approach have provided high-quality experimental data of soil-piled structure interactions in dry sand, demonstrating the role of structure stiffness on head load transfer among piles and the subsequent impact on pile shaft resistance with tunnel volume loss. This paper extends the experimental data set with a finite element numerical analysis of the problem, providing additional insights into the complex interactions. An advanced hypoplastic constitutive model was adopted for the soil and, to enable appropriate comparison of numerical and experimental results, the conditions within the centrifuge tests

*Corresponding author
Email addresses: geyang.song@eng.ox.ac.uk (Geyang Song), alec.marshall@nottingham.ac.uk (Alec M. Marshall)

were replicated numerically. Despite some discrepancies between numerical and experimental results, in particular related to limitations of the adopted soil-pile interface model, results from the numerical simulations are shown to broadly agree with the centrifuge test data. Numerical analysis results are used to explore the effect of tunnelling on pile settlements and the development of radial stresses around piles, as well as the stress paths at the soil-pile interface. These data provide additional insights to complement and extend current understanding of the complex soil-pile interactions taking place.
Keywords: Tunnelling, finite element analysis, pile, structure

Highlights

- Effect of tunnelling on piled structures.
- Numerical analysis is used to explore the pile settlement.
- Development of radial stress around piles with tunnelling.
- Stress path of soil element close to the pile with tunnelling.

1. Introduction

Piles are used to support a variety of infrastructure systems. Tunnel excavation in highly congested cities can often take place close to existing piled foundations, with associated ground movements and stress relief affecting the equilibrium state of the existing piles. This may cause pile settlements, uneven settlement among pile groups, or pile distress beyond design specifications (Kaalberg et al., 2005; Selemetas, 2005; Jacobsz et al., 2004; Lee and Chiang, 2007; Marshall and Mair, 2011; Ng et al., 2013, 2014; Williamson et al., 2017a,b; Franza and Marshall, 2019; Franza et al., 2021a; Loganathan et al., 2000; Wang et al., 2020; Franza et al., 2021a,b). These studies have demonstrated the importance of understanding the influence of tunnel excavation on pile resistance.

Geotechnical centrifuges have been widely used as a tool to investigate tunnel-pile-structure interaction (TPSI) problems. In these studies, piles are generally individually loaded or rigidly connected via a pile cap to investigate the tunnel-pile-structure interaction problems (Loganathan et al. (2000); Lee and Chiang (2007); Boonsiri and Takemura (2015); Wang et al. (2020)). However, these methods neglect or overestimate the effect of structure stiffness, which could affect the load transfer among the piles during tunnel volume loss, and consequently change the shaft resistance along the piles. Recent developments at the University of Nottingham Centre for Geomechanics (NCG) have incorporated a hybrid approach to modelling the tunnel-building interactions using the so-called Coupled Centrifuge-Numerical Modelling (CCNM) application (Idinyang et al., 2018a,b; Franza and Marshall, 2019), wherein the tunnel, soil, and piles are modelled in the centrifuge, a connected building is simulated numerically, and data related to pile displacements and loads are transferred in real-time between the centrifuge and numerical domains. The approach accurately accounts for vertical pile head load redistribution during tunnel volume loss (which depends on the characteristics of the modelled building), updates the pile head loads applied in the centrifuge as the test progresses, and provides a high-fidelity simulation of the global tunnel-pile-structure interaction problem. Song and Marshall (2020b) used the CCNM application to model the interaction between tunnel volume loss and piles connected to a five-storey steel frame structure and demonstrated the significance of the structure effect on pile resistance.

Numerical models have also clearly made important contributions to developing our understanding of tunnel-pile and tunnel-pile-structure interactions. Many numerical investigations have made use of available centrifuge test data as a means of verifying the numerical models (Hong et al., 2015; Ng et al., 2015; Soomro et al., 2018; Li and Zhang, 2020; Cheng et al., 2007; Wang et al., 2020). The numerical analyses typically adopt pressure or displacement controlled methods to simulate the tunnel volume loss process. In some instances, the mode of volume loss simulation is guided by the type of model tunnel used in the centrifuge tests against which the numerical models are compared; a fluid-filled flexible membrane model tunnel is arguably best suited to a pressure-controlled (or material softening (Li and Zhang, 2020)) simulation, whereas a displacing rigid-boundary model tunnel is well replicated by a displacement controlled simulation. There are studies which have adopted simulations which go against the above logic that have successfully demonstrated agreement between numerical and centrifuge test results

(Cheng et al., 2007; Hong et al., 2015; Soomro et al., 2018; Wang et al., 2020). The study conducted by Song and Marshall (2020a) investigated the implications of the use of the different model tunnel types using centrifuge and numerical modelling data. In common with the centrifuge tests, numerical models also typically assume either a free pile head or one where the pile is rigidly connected to a pile cap; the effect of global structure stiffness on pile loading and displacement is not considered. As a result, there is a lack of detailed numerical simulation of tunnel-pile-structure interaction where the effect of structure stiffness is included.

In this paper, an advanced hypoplastic constitutive model is employed within the finite element analysis (FEA) software ABAQUS (Hibbitt, 2002) to simulate the tunnel-pile-structure interaction centrifuge tests reported by Song and Marshall (2020b), which used the CCNM application to account for the effect of building stiffness on pile head load redistribution during tunnel volume loss. The displacement controlled method was used in the numerical simulations to replicate the deformed shape of the eccentric rigid boundary mechanical (eRBM) model tunnel used in the centrifuge tests. A comparison is made between the numerical and centrifuge test results, focusing on pile settlements and load transfer between piles, with limitations of the adopted soil-pile interface model also discussed. Despite some discrepancies between numerical and experimental results, sufficient confidence was achieved in the adopted numerical simulation for the soil-structure interaction analysis within dry sand. The numerical model is then used to extend the understanding of the complex soil-pile interactions, investigating elements that could not be easily measured experimentally, such as soil settlements and radial stress development around the piles, as well as the stress paths at the soil-pile interface.

2. Centrifuge modelling

Two centrifuge tests are reported in this paper: (1) a tunnel-pile group interaction (TPGI) test and (2) a tunnel-pile-structure interaction (TPSI) test. These tests were previously reported in Song and Marshall (2020b); readers can refer to that paper for a more in-depth description of the equipment and test methodology.

The centrifuge tests were conducted on the NCG 2 m radius, 50 g-ton geotechnical centrifuge at an acceleration of 80 times gravity. Figure 1 shows the layout of the two centrifuge tests. In test TPGI, four piles were individually loaded, and the pile head load did not change with tunnel volume loss. In test TPSI, piles were virtually connected to a 5-storey steel frame structure using the CCNM application (Idinyang et al., 2018a,b; Franza and Marshall, 2019) (more details provided later).

2.1. Centrifuge model

The centrifuge container has internal dimensions of 150 mm width, 700 mm length, and a height of 400 mm. The model tunnel had an initial diameter of D_t=90mm and was buried with a cover distance C=162 mm, giving a cover to diameter ratio of C/D_t=1.8.

An eccentric rigid boundary mechanical (eRBM) model tunnel (Song et al., 2018; Song and Marshall, 2020a) was used in the centrifuge tests to simulate tunnel volume loss. The eRBM model tunnel consists of six tunnel segments that represent the tunnel boundary. A bi-directional screw shaft

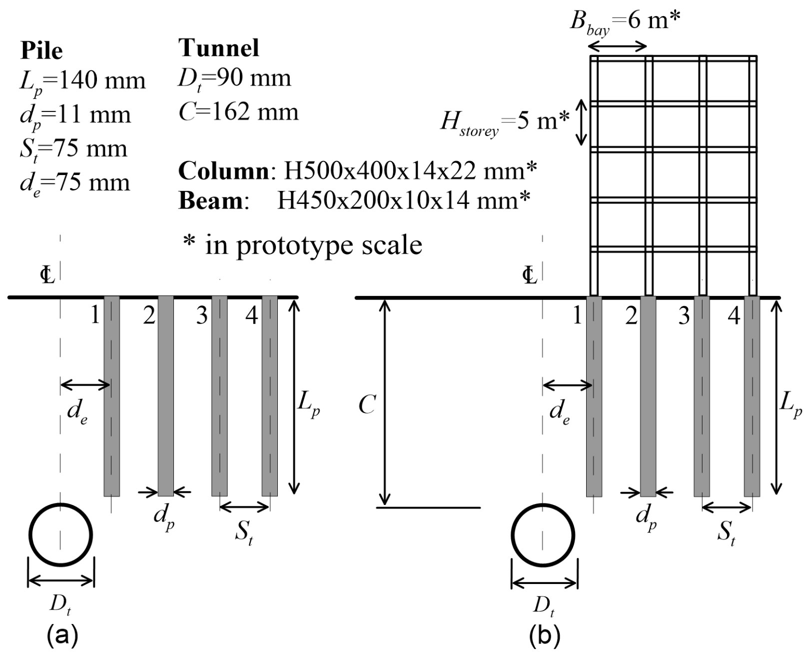

Figure 1: Test layout of the centrifuge tests (a) TPGI, and (b) TPSI

drives the six segments, which displace inwards at varying levels with rotation of the screw shaft to produce an eccentric profile of displacement around the tunnel boundary, with maximum displacement at the tunnel crown and zero displacement at the invert. A detailed description of the model tunnel configuration is provided in Song and Marshall (2020a).

In test TPGI, designated working loads were applied to each of the piles and maintained constant throughout the tunnel volume loss process using a load control system. In test TPSI, the same working loads were initially applied to the piles, after which the load control of the piles was passed over to the CCNM application, allowing the ABAQUS numerical simulation to adjust pile head loads during the tunnel volume loss process (Franza and Marshall, 2019). In both tests, tunnel volume loss was increased in small increments of ≈0.1%; subsequent increments of volume loss were only allowed after achieving a 'stable state' and acquiring all necessary data. This 'stable state' is most relevant to the TPSI test where, for a given increment of volume loss, pile head displacements are passed to the numerical model of the connected structure through the real-time interface of the CCNM application (Idinyang et al., 2018a), which calculates new pile head loads depending on the magnitude of pile settlement and the characteristics of the building. The adjusted pile head load is then passed back to the centrifuge through the CCNM application, which may cause subsequent small changes in pile head displacements, requiring another 'loop' of the CCNM process. This 'loop' is repeated until the 'stable state' is achieved, based on a requirement for sufficiently small changes in pile head load and displacements.

A linear elastic five-storey steel frame structure was simulated in the ABAQUS numerical model, with a Young's modulus of $E = 210\,\text{GPa}$ and a Poisson's ratio of $\mu = 0.3$; the sizes of the columns and beams are given in prototype scale in Figure 1. Based on Eurocode specifications (Gulvanessian et al., 2009), the total prototype scale pile head load applied to the two inner piles was 2364 kN, and 1630 kN for the two outer piles.

2.2. Model piles and strain sensors

The model piles were made from hollow aluminium tube with an outer diameter of 10 mm and a thickness of 1 mm, giving an axial stiffness $EA = 19.4 \times 10^3\,\text{MN}$ in prototype scale. In practice, a 0.8 m diameter concrete pile has an axial stiffness $EA = (10 - 14) \times 10^3\,\text{MN}$, which is slightly lower than the model pile. Piles had sand grains (the same sand used for soil body) bonded to the outer surface of the pile to create a fully rough interface. The final pile diameter was d_p=11 mm.

Optical Fibre Bragg Grating (FBG) sensors were used to measure strains at localised locations along the piles (Song et al., 2021), allowing calculation of the distribution of pile shaft resistance. The FBG sensors were made from a single-mode optical fibre. Two fibres, each containing three FBG sensors (corresponding to strain measurement locations), were installed along opposing inner surfaces of the model piles, with measurement locations at 40, 85 and 130 mm below the ground surface. The model piles were calibrated on a loading frame within a temperature-controlled room, providing a reliable linear relationship between FBG wavelength shift and applied load (i.e. calibration factor).

2.3. Model preparation and testing procedure

Fine-grained silica sand commonly known as Leighton Buzzard Fraction E sand was used for the tests. The sand has a typical average diameter D_{50} of 0.14 mm, specific gravity G_s of 2.65, and was prepared by dry sand pouring. The model preparation procedure can be briefly summarised as follows. One end of the eRBM model tunnel was fixed within the back wall of the strongbox, which was laid horizontally (the model tunnel oriented upwards), and a temporary wall secured at the location corresponding to the intended soil surface. The sand was poured in the direction of the tunnel longitudinal axis to achieve a relative density (I_d) of 90%. After sand pouring, the strongbox was rotated to its upright position and the temporary wall removed (revealing the soil surface). The four piles were then pushed into the sand at 1 g using a frame to ensure the piles were pushed vertically at the designated location and to the required depth. The pile loading actuators were then connected to the piles.

The centrifuge testing procedure can be briefly summarised as follows. A constant 5 N vertical load (model scale) was applied to the piles and maintained during centrifuge spin-up to 80 g (done to try to minimise relative soil-pile displacements during the spin-up process). Three stabilisation cycles were performed (going from 80 g to 10 g and back to 80 g; done to encourage uniform stress conditions within the models and improve repeatability of tests). After these cycles, the pile loading and volume loss processes, as previously described, were performed.

3. Finite element simulation

Finite element models were developed to simulate the TPGI and TPSI centrifuge tests using the user-defined hypoplastic constitutive model developed by von Wolffersdorff (1996) to model the soil.

3.1. Element mesh and boundary conditions

Figure 2 shows the finite element mesh for test TPSI. The intention of the analysis was to simulate the centrifuge tests as closely as possible. Therefore, the dimensions of the numerical model match exactly with the centrifuge test. An eccentric displacement control method was used to simulate the eccentric rigid boundary mechanical (eRBM) model tunnel used in the centrifuge tests (Song and Marshall, 2020a). In this method, the rigid tunnel boundary is divided into six segments and pre-defined radial displacements are imposed for each segment to generate a non-uniform radial displacement around the tunnel. Figure 2 shows the radial displacement of each segment at a tunnel volume loss of $V_{l,t} = 3\%$. Solid elements (C3D8) were used to model the soil, pile and rigid tunnel boundary. Beam elements (B31) were used to model the steel frame structure. The coefficient of lateral earth pressure was assumed to be $K_0 = 0.5$. A fixed boundary was used along the bottom of the mesh, vertical roller boundaries were used on the sides of the mesh, and no constraints were applied to the ground surface. Element size was determined using a procedure whereby a further decrease in element size had a negligible effect on soil settlement with tunnel volume loss (based on the greenfield tunnelling condition).

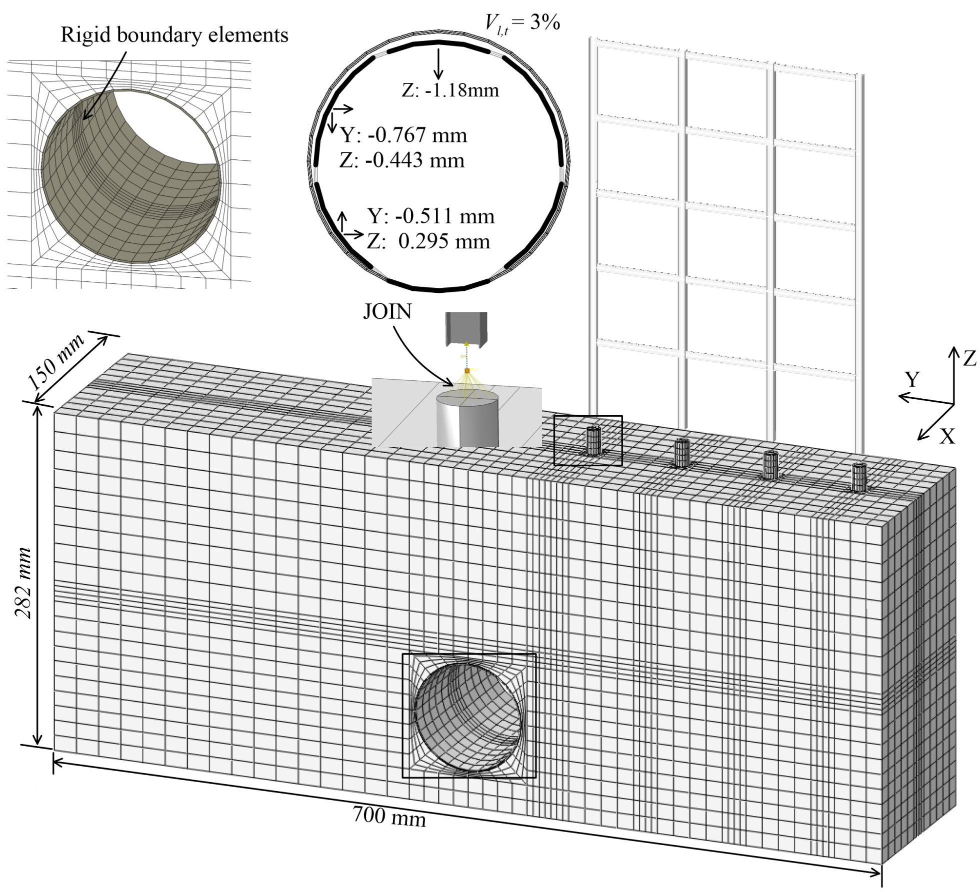

Figure 2: Finite element mesh for test TPSI

3.2. Constitutive model and model parameters

The basic hypoplastic model was adopted in this study, which consists the following 8 parameters: critical state friction angle ϕ'_c, granular hardness h_s, fitting parameter n, minimum/maximum/critical void ratio at zero pressure $e_{d0}/e_{i0}/e_{c0}$, and $\alpha;\beta$ which govern the stiffness of the soil. The hypoplastic model parameters for Leighton Buzzard Fraction E sand were obtained and calibrated using oedometer and triaxial tests data from Song and Marshall (2020a). Note that parameters α and β calibrated by Song and Marshall (2020a) were based on stress-strain data from two drained triaxial compression tests where the axial strain data was obtained from an external linear variable differential transformer (LVDT). Jardine et al. (1984) indicated that the use of external LVDTs provides insufficient accuracy for stiffness measurement in the triaxial test. Therefore, for this paper, local LVDT data from the two drained triaxial compression tests were used to re-calibrate the parameters α and β. Figure 3 shows the stress-strain behaviour from the two triaxial tests using both local and external LVDT data, as well as the finite element simulation result using α=0.08 and β=1.5. Note that, despite the slight over-prediction of the peak deviator stress for the FEA, the simulation replicates the soil stiffness within the small strain range (axial strain less than 0.5%) very well, which is of primary concern for the numerical analysis of tunnel construction processes (Addenbrooke et al., 1997). Table 1 summarises the modified model parameters adopted in this study (after Song and Marshall (2020a)).

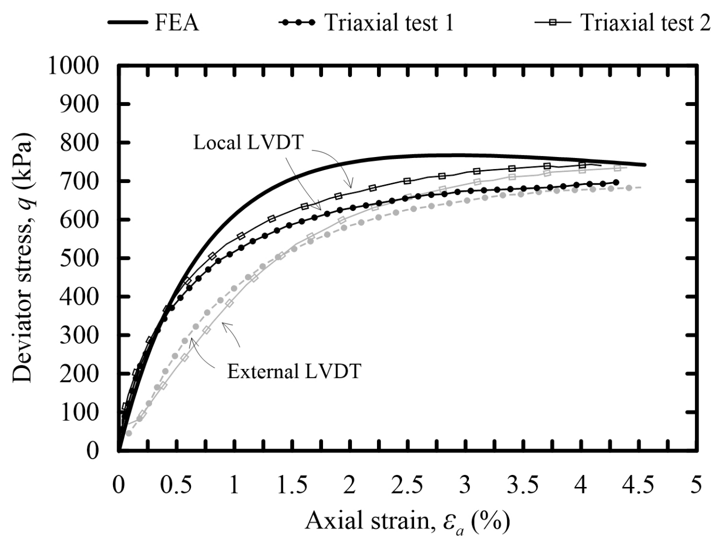

Figure 3: Triaxial test calibration

Table 1: Adopted hypoplastic model parameters for Leighton Buzzard Fraction E sand, after Song and Marshall (2020a)

Parameter	Value	Source
Critical state friction angle ϕ'_c	32°	Heap test
Granular hardness h_s	1969 MPa	Oedometer test
Exponent n	0.447	Oedometer test
Minimum void ratio at zero pressure e_{d0}	0.624	Herle and Gudehus (1999)
Critical void ratio at zero pressure e_{c0}	1.16	Oedometer test
Maximum void ratio at zero pressure e_{i0}	1.392	Herle and Gudehus (1999)
Exponent α	0.08	Triaxial test* $I_d = 90\%$
Exponent β	1.5	Triaxial test* $I_d = 90\%$

* Based on local LVDT measurements

3.3. Numerical modelling procedure

The numerical model is intended to simulate the conditions within the centrifuge tests as closely as possible, for example, self-weight of the pile, the effect of increasing gravity level from 1 g to 80 g, the tunnel volume loss process, and the effect of the connected steel frame structure. Note that the frame structure is weightless in the numerical model; the weight of the structure as well as the working loads applied were calculated based on Eurocodes (discussed previously) and imposed to the pile heads (total pile head load).

For gravity increase (spin-up) simulation, it was found that replicating the full 1 g to 80 g process caused instabilities within the numerical simulations during the tunnel volume loss stage, preventing analysis of the full centrifuge test. By replicating from 2 g to 80 g, the numerical analyses could simulate the full experimental volume loss range (up to tunnel volume loss $V_{l,t} = 3\%$). Results presented in this paper therefore relate to models that replicated the 2 g to 80 g process; Song and Marshall (2020a) indicated that the difference in ground settlements at a given tunnel volume loss was negligible between the '1-80 g' and '2-80 g' simulations.

The soil-pile interface for the finite element analyses was simulated using a Coulomb friction law, in which the friction coefficient was set to be $\tan(\phi'_c)$=0.62 (matching the rough pile interface from the centrifuge tests where sand was bonded to the exterior of the piles). An absolute elastic slip distance (1.5 mm) was used to define the tangential behaviour of the soil-pile interface, which is based on centrifuge pile jacking tests reported by Song and Marshall (2020b).

To replicate the non-uniform radial displacement of the eRBM model tunnel in the centrifuge (Song and Marshall, 2020a), a rigid boundary mesh was implemented (see Figure 2) with a non-uniform displacement profile. The interface between the soil and the rigid boundary was simulated using a Coulomb friction law with the assumption that the soil-tunnel boundary interface behaved in the same way as the pile-soil interface. In terms of the steel frame structure simulation for test TPSI, the same model used in the TPSI centrifuge test (with the CCNM application) was adopted in the numerical simulation. Note that, in both centrifuge and FEA tests, only vertical loads were transferred between the building frame and the piles, neglecting the effect of lateral and rotational degrees of freedom; Franza and Marshall (2019) demonstrated that the vertical degree of freedom has the dominant role for this considered scenario.

The finite element analysis procedure can be summarised as follows. An initial soil stress profile was imposed on the soil elements, where the static earth pressure coefficient was set to $K_0 = 0.5$ and the soil stresses calculated for an acceleration field of 2 g. Then, a geostatic step was conducted to ensure the soil displacements were reset to zero (the maximum soil displacement after this geostatic step was found to be 2×10^{-5} mm). Soil elements inside the tunnel were then removed and tunnel boundary elements were added to the model, with the Coulomb friction law interface activated at the soil-tunnel boundary interface. Soil elements at the pile locations were removed and the model piles added, followed by the activation of the soil-pile interface (Coulomb friction law). For the TPGI FEA test, a 5 N load was then applied to the piles (as in the centrifuge test). For the TPSI FEA test, piles were first loaded to 5 N, then the steel frame structure (which is weightless) was added to the model. In the TPSI centrifuge test, a hinged joint was used between the base of the columns and the pile heads, transferring only vertical loads between the columns and piles. This simplification was adopted because the real rotational stiffness at this connection is not known. Franza and Marshall (2019) illustrated that the influence of this pile-structure connection is minor for framed buildings with isolated pile heads, as is the case in this study, hence the impact of this assumption is minimal. For the real-time data interface (Idinyang et al., 2018a), only vertical pile displacements and vertical pile head loads were shared between the geotechnical (centrifuge) and structural (numerical) domains. In the TPSI FEA test, the four piles were connected to the steel frame structure via a pin joint. This pin joint connection was achieved using the ABAQUS connection type JOIN with a restriction of displacements in the X and Y directions as well as the rotation along the Y and Z axes (see Figure 2 for the coordinate system). Therefore, only vertical displacements and vertical forces were translated between the piles and the structure. The base of the structure columns were free to rotate, which depends on the global deformation of the structure (identical to the TPSI centrifuge test).

Once the structure was connected to the piles via this pin joint, the gravity level of the entire model was increased from 2 g to 80 g [within one step (252 increments) within ABAQUS], during which time the tunnel boundary was fixed in terms of distortion (change in shape) and translation (rigid body motion). Piles were then loaded to the designated working load (255 N for exterior piles 1 and 4, and 370 N for interior piles 2 and 3). Finally, a non-uniform displacement profile (discussed above) was imposed on the rigid boundary elements to simulate tunnel volume loss. For the TPGI FEA test, pile head load was kept constant, whereas for the TPSI FEA test, pile head load varied with tunnel volume loss as it was affected by the structure stiffness.

4. Results

4.1. Spin-up effect on pile shaft resistance

For the centrifuge tests, a 5 N pile head load was maintained during centrifuge spin-up (from 1 g to 80 g). The increase in self-weight of the soil will cause relative displacements between the piles and the adjacent soil. To better understand the spin-up effect, Figure 4 shows the pile settlement after gravity increase in the centrifuge and FEA TPGI tests. Both tests show comparable pile settlement after spin-up, however the FEA pile settlement increases with pile number (i.e. with distance from the tunnel, refer to Figure 1), a consequence of the fixed tunnel boundary, whereas Pile 1 (nearest the tunnel) shows the largest settlement in the centrifuge test, indicating that some movement of the model tunnel likely occurred during spin-up. Figure 4 (a) also shows the soil settlement adjacent to the piles at their centreline along the depth of piles for the FEA test which demonstrates that the adjacent soil settlement was more than the pile settlement near the upper portion of the piles but was similar in magnitude near the lower portion of the piles (comparative centrifuge test data is not available), indicating that the near-surface soil acts to drag down the piles.

Figure 4 also shows the axial force along the piles during spin-up for FEA

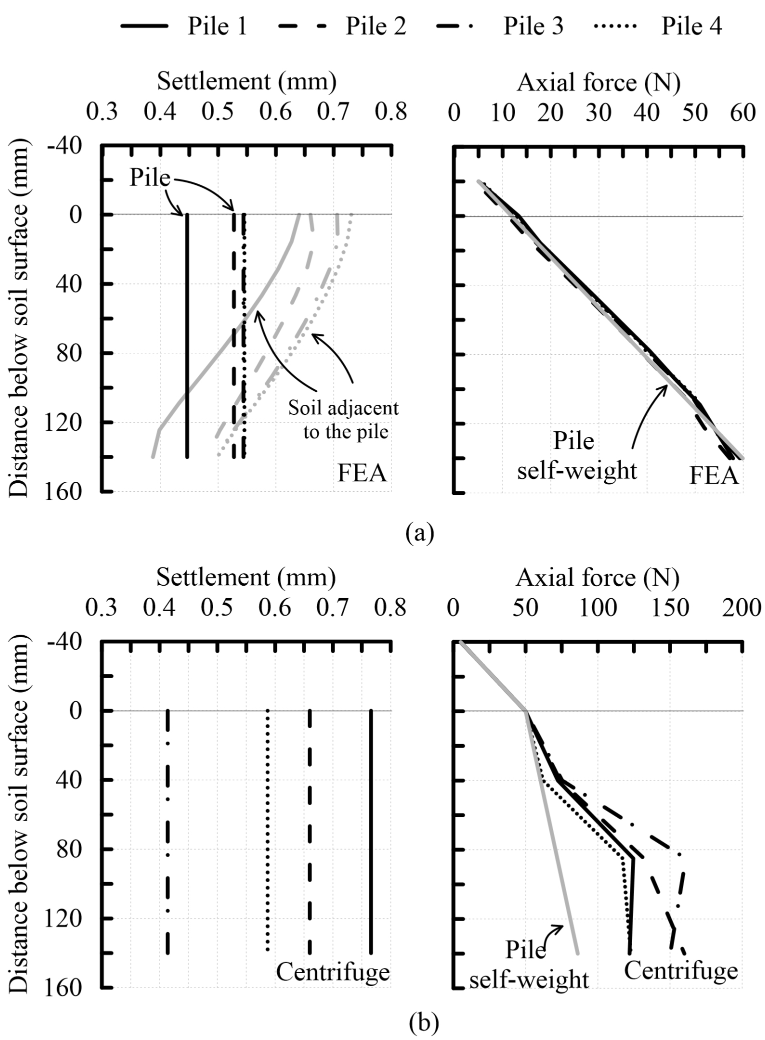

Figure 4: Displacement and axial force along the pile after spin-up: (a) finite element analysis, (b) centrifuge test

and centrifuge tests. The solid grey line represents the pile's self-weight at 80 g (the 5 N pile head load is included). Centrifuge test data show an increase in axial force along the pile after spin-up (axial force along the pile is greater than the pile self-weight), resulting from the drag-down forces applied by the soil to the pile shaft due to relative soil-pile movement. The pile axial forces from the FEA match closely to the pile self-weight, indicating an insignificant change in shaft resistance during spin-up. Shaft resistance mobilisation is governed by (1) the magnitude of relative displacement between the soil and pile, and (2) the magnitude of effective radial stress (σ'_r) around the pile. In relation to (1), Song and Marshall (2020b) used a camera to measure the soil settlement (75mm away from the pile at the front transparent wall of the centrifuge container) along the depth of the piles during centrifuge spin-up. Results indicated a maximum relative soil-pile displacement in the centrifuge test of around 1 mm, which is greater than the numerical simulation result presented in Figure 4 (a) (maximum relative displacement of around 0.2 mm).

In relation to (2), Figure 5 shows the average effective radial stress ($\sigma'_{r,ave}$) along the depth of pile 1 after spin-up (2-80 g) in the TPSI FEA test. The $\sigma'_{r,ave}$ value was calculated as the average effective radial stress around the pile circumference. In addition, the static earth pressure is presented ($\sigma'_{r,ave}/\sigma'_v$=0.5). FEA results show that the static earth pressure condition remains valid along the pile, indicating that the shaft resistance mobilisation was very limited. For the centrifuge test, due to the relatively larger movement between the soil and piles, Song and Marshall (2020b) indicated that the static earth pressure coefficient is no longer valid and, based on the radial stress measurement data given by Jacobsz (2003), suggested that $\sigma'_{r,ave}/\sigma'_v$ close to the pile after centrifuge spin-up was about 1.46 (see Figure 5). This difference in $\sigma'_{r,ave}$ between the FEA and centrifuge tests would significantly affect the axial force (mobilised shaft friction) along the pile during spin-up.

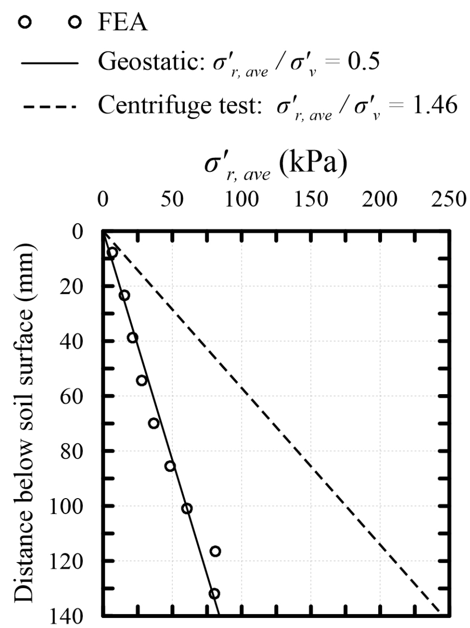

Figure 5: Average radial stress $\sigma'_{r,ave}$ after spin-up

4.2. Pile loading

After spin-up, piles were loaded to the designated working load (255 N for outer piles 1 and 4; 370 N for inner piles 2 and 3). Figure 6 shows the axial force along the piles before and after pile loading for test TPSI in both centrifuge and FEA tests.

For the centrifuge test, the pile end bearing load was not measured directly; it was approximated by linearly extrapolating the data from the two closest FBG measurement points (Figure 6 illustrates the locations of the two measurement points used in the extrapolation). All piles in both centrifuge and numerical tests show an increase in axial force along the entire pile length due to pile loading. For the piles in the centrifuge test, the increase in pile end bearing load is much smaller than the applied head load, indicating that the pile shaft resistance took most of the applied load. For the numerical simulation, the majority of the applied pile load was taken by the pile end bearing load.

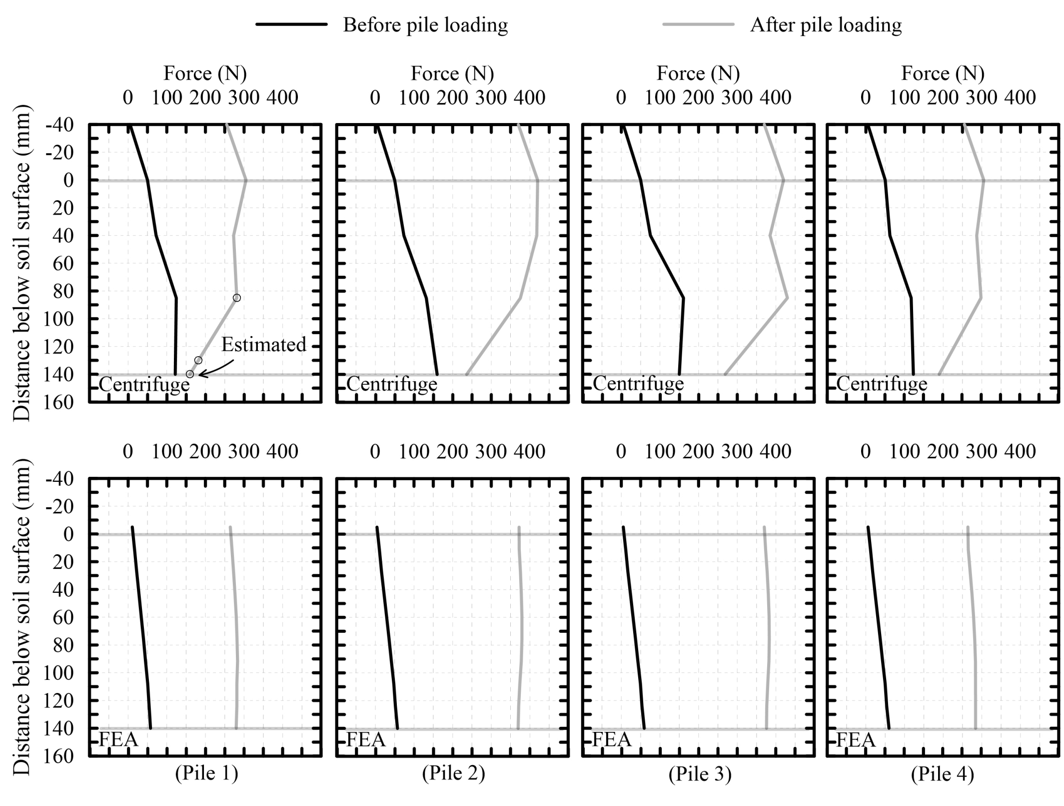

Figure 6: Pile axial force after pile loading for centrifuge and FEA test TPSI

To further understand the development of shaft resistance caused by pile loading, Figure 7 shows the shaft resistance along the piles before and after pile loading in test TPSI. Note that, for the centrifuge tests, since there are only three measurement points along the depth of the piles, the shaft resistance between two measurement points is presented as a constant value (average shaft resistance between two measurement points), which results in some relatively large 'jumps' in shaft resistance in Figure 7. Prior to pile loading (after spin-up), negative pile shaft resistance developed along most (centrifuge) and all (FEA) of the lengths of the piles, indicating that the soil was pulling the pile downwards (as previously discussed). Note, however, the difference in magnitude between centrifuge and FEA results, with peak negative shaft resistance being about -40 kPa in the centrifuge test, compared to peak values of about -10 kPa from the FEA results. After pile loading, both centrifuge and numerical simulation results show an increase in shaft resistance which, for both centrifuge and FEA, occurs mainly near the base of the piles, where shaft friction changes from negative to positive. In the centrifuge, after pile loading, the full length of most piles (apart from the middle portion of piles 3) are noted to have positive shaft resistance, whereas for some of the piles in the FEA tests, the shear resistance in the upper portion of the piles remained negative (the pile head load was insufficient to cause a reversal of shear stress direction). The difference in magnitude of change in shaft resistance between centrifuge and FEA results is significant, with large increases of about 80 kPa taking place in the centrifuge (carrying most of the applied pile head load, as previously noted), compared to about 15 kPa for FEA (where most of the applied load was carried by the pile base load).

Overall, these results indicate that the FEA model did not fully capture the load distribution within the piles during pile loading; the FEA results show a bias for pile end-bearing resistance, whereas the centrifuge results show greater load resistance along the pile shaft. This discrepancy is, in part, a limitation of the adopted FEA soil-pile interface model (Coulomb friction law, with an absolute elastic slip distance of 1.5 mm). The use of a complex soil-pile interface model developed by Stutz et al. (2016) was also attempted in this study, however its use alongside the adopted complex constitute model for soil (required to get an accurate small-strain stress-strain response) resulted in convergence issues at most values of tunnel volume losses ($V_{l,t} > 0.5\%$). In addition, this discrepancy is also a consequence of the FEA model results from the spin-up stage, where it was shown that the lateral stresses acting on the piles in the centrifuge tests were likely considerably larger than within the FEA simulations. Nevertheless, the subsequent sections will explore how the FEA model results compare against centrifuge test data during tunnel volume loss.

4.3. Pile settlement due to tunnelling

Song and Marshall (2020b) highlighted the importance of two main mechanisms governing changes in pile response to tunnelling: Mechanism T (for tunnelling) relating to tunnelling induced ground movements, and Mechanism S (for structure) relating to load transfer between pile heads due to structure stiffness and deformation. The following discussion will also refer to these mechanisms as a means of explaining some of the observed behaviour.

Figure 8 shows the normalised pile settlement (S_p/d_p; positive settlements are downwards) with tunnel volume loss for both centrifuge and FEA

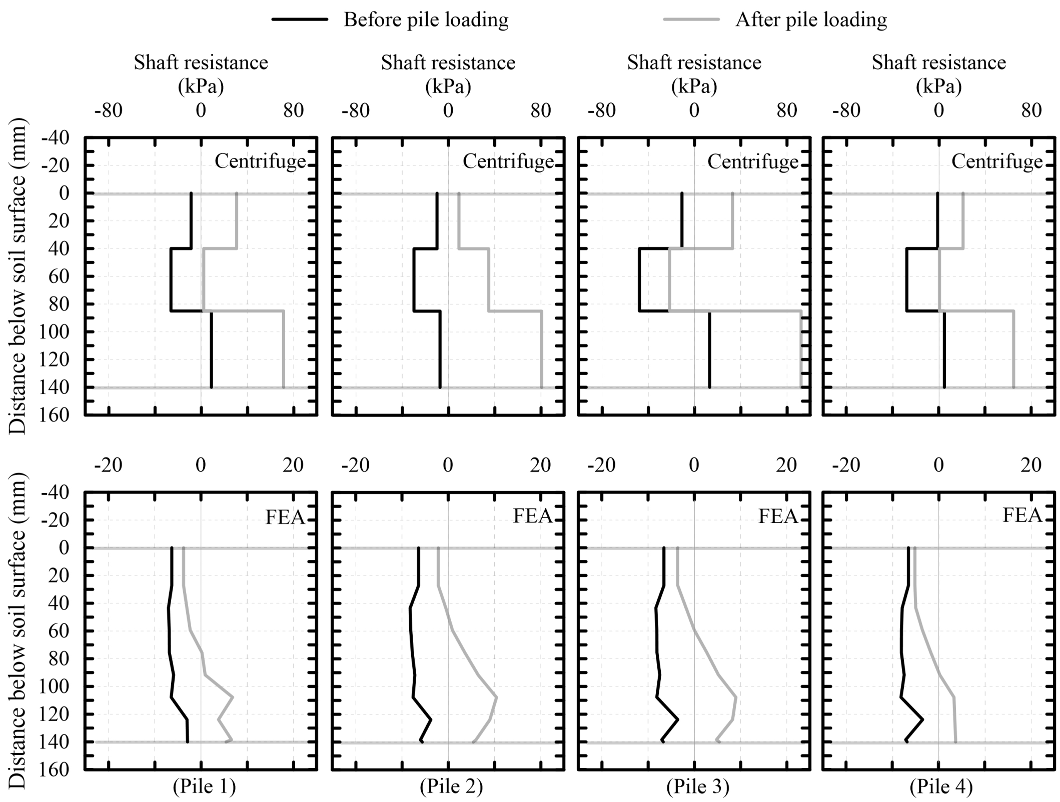

Figure 7: Shaft resistance along the pile after pile loading for centrifuge and FEA test TPSI

tests for piles 1 to 4; note that the normalised settlement scale is not consistent across all piles. For test TPGI, a constant load was maintained during the tunnel volume loss process, whereas the pile load varied in test TPSI as a result of load redistribution from the (virtually) connected five-story steel frame structure. In general, the difference between TPGI and TPSI centrifuge test results for pile displacements is relatively small, indicating that Mechanism S had a minor impact on pile settlements (for example, at prototype scale, pile 2 settlement increased from about 10 mm for TPGI to about 12 mm for TPSI at $V_{l,t} = 3\%$). This suggests that practical approaches for evaluating pile settlements caused by tunnelling (e.g. Selemetas (2005); Selemetas and Standing (2017); Devriendt and Williamson (2011)) could conveniently overlook the effects of Mechanism S without significant consequences (though pile-group effects may also be important, which are not accounted for by Devriendt and Williamson (2011); analytical methods such as Franza et al. (2021a) may provide a more robust approach for design). It should be noted, however, that the case considered here included a relatively flexible framed building. For framed buildings, where it has been shown that shear deformations dominate their response to tunnelling, Xu et al. (2020) proposed a relative soil-building shear stiffness parameter κ; for this study, a value of $\kappa > 500$ was estimated, which is greater than all cases considered within Xu et al. (2020) and indicates that the building used in this study was relatively flexible (this is due mainly to the fact that the Xu et al. (2020) buildings assumed plane-strain vertical walls running along the direction of the tunnel, whereas individual columns were considered in this study.) For less flexible structures, Mechanism S may have more of an impact on pile settlements; more study is needed to consider a wider range of relative soil-building stiffness cases.

The FEA settlements tend to over-predict centrifuge results for piles 1, 2 and 3 in both tests TPGI and TPSI. Both centrifuge and FEA results show that the pile located closest to the tunnel (pile 1) settled most with tunnel volume loss. In the centrifuge tests, the effect of the connected structure on the pile 1 settlement response to volume loss was negligible (TPGI and TPSI results being closely matched), whereas the FEA results for pile 1 show that, at higher volume losses, the TPSI settlements become less than TPGI (due to pile unloading from Mechanism S, as discussed in the next section). For pile 2, both centrifuge tests (TPGI and TPSI) show similar pile settlement initially ($V_{l,t}$ less than 1%) but diverge somewhat at higher volume losses, with TPSI settlements being slightly larger than TPGI due to increased pile head loads as volume loss increases (caused by load redistribution within the building (Mechanism S), as discussed in the next section). A similar observation is noted for the FEA results, though the difference in pile 2 settlement between TPSI and TPGI simulations is more significant than it was in the centrifuge. The response of pile 3 is similar to that of pile 2, with magnitudes of displacements being smaller. Finally, for pile 4 in the centrifuge tests, at the end of tunnel volume loss ($V_{l,t} \approx 3\%$), test TPGI shows greater settlement than test TPSI (indicating the TPSI pile head load reduced during volume loss due to Mechanism S). For the FEA TPGI test, the structure stiffness effect was sufficient to cause a negative (upwards) displacement of pile 4 for tunnel volume loss $V_{l,t} > 1.5\%$ (note, however, that the scale of pile 4 movements is very small; a 0.1% difference in S_p/d_p

corresponds to a prototype pile settlement of just under 1 mm).

In general, the FEA model provided satisfactory predictions of the pile settlements with tunnel volume loss; the magnitudes of settlements were clearly not a perfect match, however the trends in relation to associated mechanisms (i.e. pile loading/unloading during volume loss) were captured well.

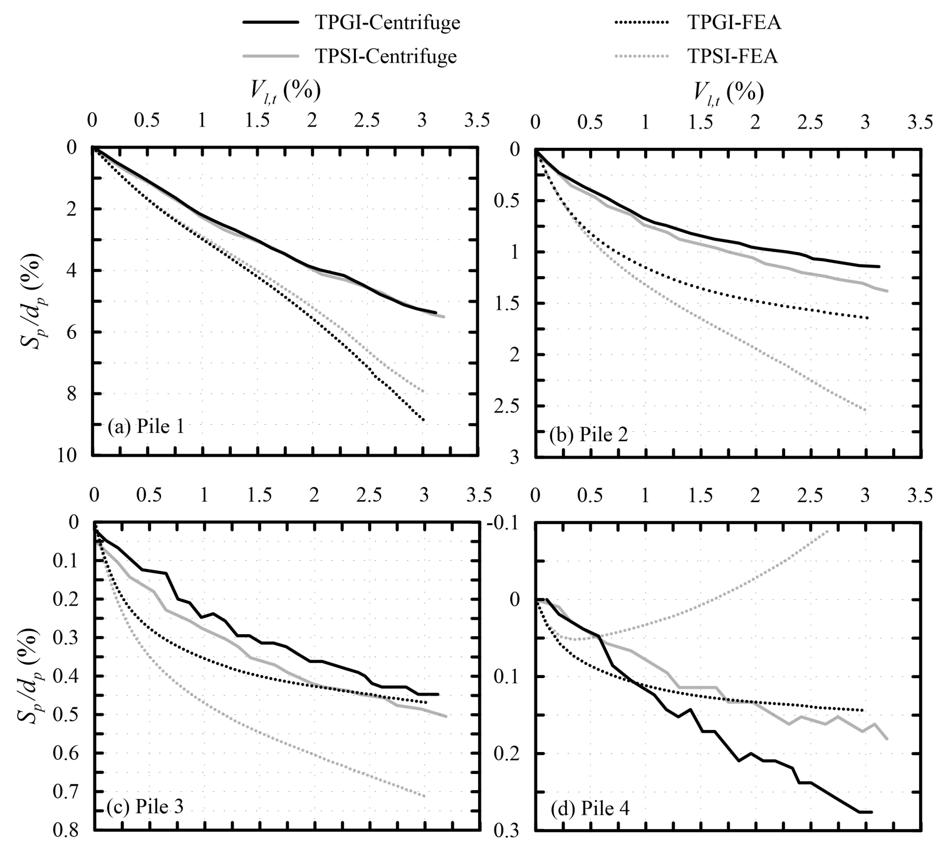

Figure 8: Normalised pile settlement (positive downwards) with tunnel volume loss for both centrifuge and FEA tests

4.4. Pile head load transfer between piles

Figure 9 shows the change in pile head with tunnel volume loss for both centrifuge and FEA tests. Pile head loads remain constant for test TPGI, hence the discussion below relates solely to test TPSI. The relative change of pile head loads is noted to be very similar in the centrifuge and FEA tests, which is a function of structural characteristics (consistent for both tests) but also the magnitude of pile settlements (which differed, as illustrated in Figure 8). Pile 1 shows a decrease in head load with tunnelling of about 50 N at $V_{l,t} = 3\%$ (≈20% reduction), which did not have a noticeable impact on the centrifuge pile settlement (Figure 8), but did have a small effect on the FEA settlements (with TPSI reducing compared to TPGI due to pile unloading). The majority of the reduced pile head load from pile 1 was transferred to the adjacent pile 2, which increased by about 65 N (≈18%) at $V_{l,t} = 3\%$ in both centrifuge and FEA tests. Pile 3 also showed an increase in head load with tunnelling by approximately 11 N (3%) in the centrifuge and 19 N (5%) in the FEA test at $V_{l,t} = 3\%$. For pile 4, due to a global rotation of the building, both centrifuge and FEA tests show a decrease in pile head load with tunnelling of ≈30 N (12%) for the centrifuge and FEA tests. Note that the net change in pile head load across the entire structure must equal zero.

These results demonstrate the importance of considering Mechanism S when evaluating pile loading within tunnel-piled structure interaction problems, even for the relatively flexible building considered in this study (more rigid structures will have a greater effect on pile head load redistribution, as demonstrated by Franza et al. (2021b)). Mechanism S is currently not considered within standard tunnel design risk assessments (e.g. Mair et al. (1996); Schoor et al. (2021)), though recent work by Franza et al. (2021b) has provided a rational approach for incorporating building stiffness within a computationally efficient two-stage model for soil-pile-structure interaction analysis.

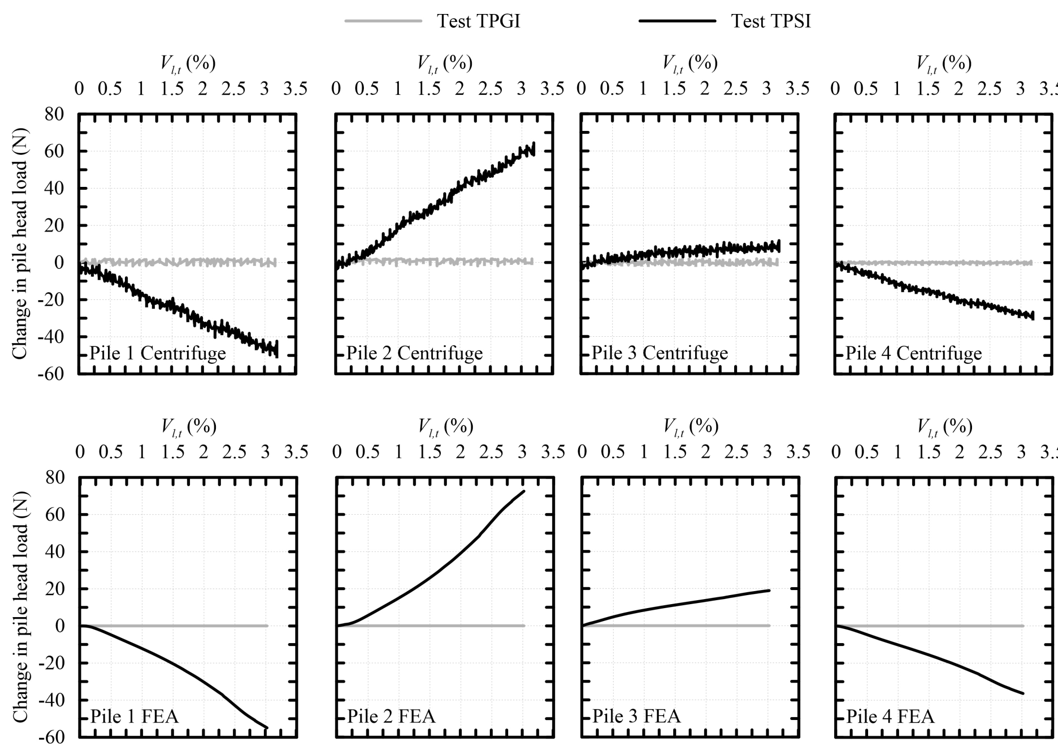

Figure 9: Pile head load with tunnel volume loss for both centrifuge and FEA tests

In general, despite the fact that the FEA test over-estimated pile settlement, the load transfer mechanism between piles agrees well between the FEA and centrifuge tests. The change in pile head load is related to the structure deformation, which is illustrated in Figure S1 in the supplemental data, showing pile settlements and the deformed structure for the centrifuge and FEA tests at a tunnel volume loss of $V_{l,t} = 3\%$. Figure S1 illustrates that that the degree of structure deformation in the FEA test was greater than in the centrifuge test.

4.5. Force distribution along piles with tunnelling

To illustrate the effect of Mechanisms T and S on the force distribution along the piles, Figure 10 plots the axial force along the depth of the piles prior to and after tunnel volume loss ($V_{l,t} \approx 3\%$) for tests TPGI and TPSI in both centrifuge and FEA tests. For pile 1 in test TPGI (constant pile head load), both centrifuge and FEA tests show that pile end-bearing force reduces with tunnelling, with additional shaft resistance being mobilised (to maintain equilibrium) with pile settlement (see Figure 8). The FEA TPGI test results for piles 2-4 show little to no effect of tunnel volume loss. For the centrifuge TPGI results, piles 2 and 3 show little change after volume loss (pile 2 shows a small increase in end-bearing load), however the data indicate that the end-bearing load in pile 4 reduced as a result of tunnel volume loss. As discussed in Song and Marshall (2020b), the reason for the reduction in end-bearing load in pile 4 is not clear, but may be due to some pile-pile interactions or boundary effects. In general, for test TPGI, as the structural stiffness effect (mechanism S) is not considered and the axial force distribution along the piles is only affected by tunnelling (mechanism T), both centrifuge and FEA tests show that the pile located closest to the tunnel experienced the most significant change in axial force. For piles located further away from the tunnel, the effect of tunnelling on pile axial force is not significant.

For test TPSI, due to mechanism S, pile 1 head load decreased by approximately 45 N and 55 N (17% and 22%) at $V_{l,t} \approx 3\%$ in the centrifuge

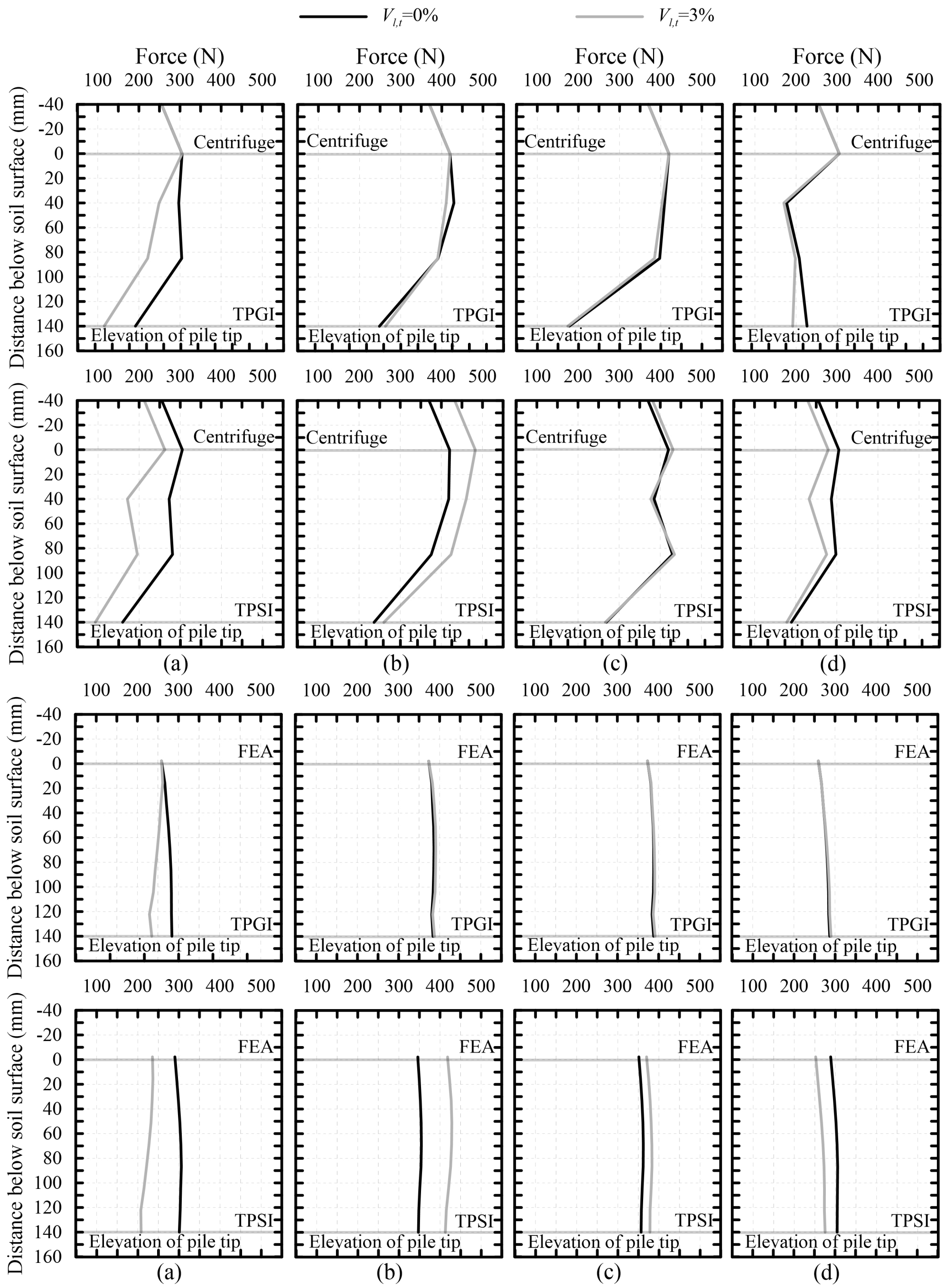

Figure 10: Pile axial load at $V_{l,t} = 0$ and 3% for both centrifuge and FEA tests: (a) pile 1, (b) pile 2, (c) pile 3, (d) pile 4

and FEA tests, respectively. Despite the decrease in pile head load, the pile end-bearing load also decreased as a result of tunnel volume loss, by a magnitude similar to pile 1 in test TPGI. In both centrifuge and FEA tests, the magnitude of decrease of the end-bearing force is greater than the decrease in pile head load, indicating that the pile shaft resistance increased. For pile 2 in test TPSI, due to mechanism S, head load increased in both centrifuge and FEA tests by about 65 N (18% increase); in the centrifuge, this added load was distributed to the pile tip (24 N; 37% of added load) and shaft (41 N; 63% of added load), whereas for the FEA, almost all of the added load was taken by the pile tip. For pile 3 in test TPSI, centrifuge test results show minimal change in pile axial force profile with tunnel volume loss, whereas FEA results show a small increase in pile head load and end-bearing load (load transferred to pile tip, as was the case for pile 2). For pile 4, both tests show a decrease in pile head load (mechanism S); FEA results show that the decreased pile head load was transferred to pile tip, whereas centrifuge results show a decrease in both shaft resistance and end-bearing load. In general, the magnitude of changes in axial forces along the piles from the numerical simulation and centrifuge tests broadly agree, and the trends of changes with tunnel volume loss agree well.

4.6. Relative pile-soil settlements with tunnelling

Axial force distributions along the piles presented in Figure 10 demonstrate that the shaft resistance along the piles changes with tunnel volume loss. The mobilisation of shaft resistance is caused by relative settlement between the soil (S_v) and pile (S_p). For centrifuge tests TPGI and TPSI, this relative settlement can be approximated using soil settlements (S_v) obtained (using image analysis techniques) at the the front acrylic wall of the centrifuge container at locations corresponding to the piles. However, this approximate approach can not fully represent the soil settlements around the pile circumference. The results of the numerical simulations, which provide detailed results of soil settlements around the piles, can be used to investigate the relative pile-soil settlements during tunnelling.

Figure 11 presents the numerical results for settlement of piles (S_p) and the surrounding soil (S_v), along the circumference of the piles, at a tunnel volume loss of $V_{l,t} = 3\%$ for the TPGI and TPSI tests. Three soil depths are shown: the soil surface, 63 mm and 125 mm below the soil surface (upper, middle, and lower rows of plots in Figure 11); theses three depths are used to represent settlements in the upper, middle and lower portions of the piles, respectively. The size of the circle represents the magnitude of the settlement, with labels indicating the scale of settlement. As the piles are relatively rigid, pile settlement is constant with depth, whereas soil settlement varies with depth.

For pile 1 (closest to the tunnel), both TPGI and TPSI tests show that the pile settlement is greater than the surrounding soil. Also, pile 1 settlement in test TPGI is greater than TPSI, resulting from the reduction of pile head load in test TPSI, whereas soil settlements for the two tests is very similar. The soil settlement around pile 1 is not uniform; all three depths show that the soil closest to the tunnel (0°) settled more than the soil on the opposite side (180°), with the disparity increasing with depth. The magnitude of soil settlement (size of the circle) increases with depth, indicating lower soil-pile relative settlements at greater depth. In general, the pile 1 settlement

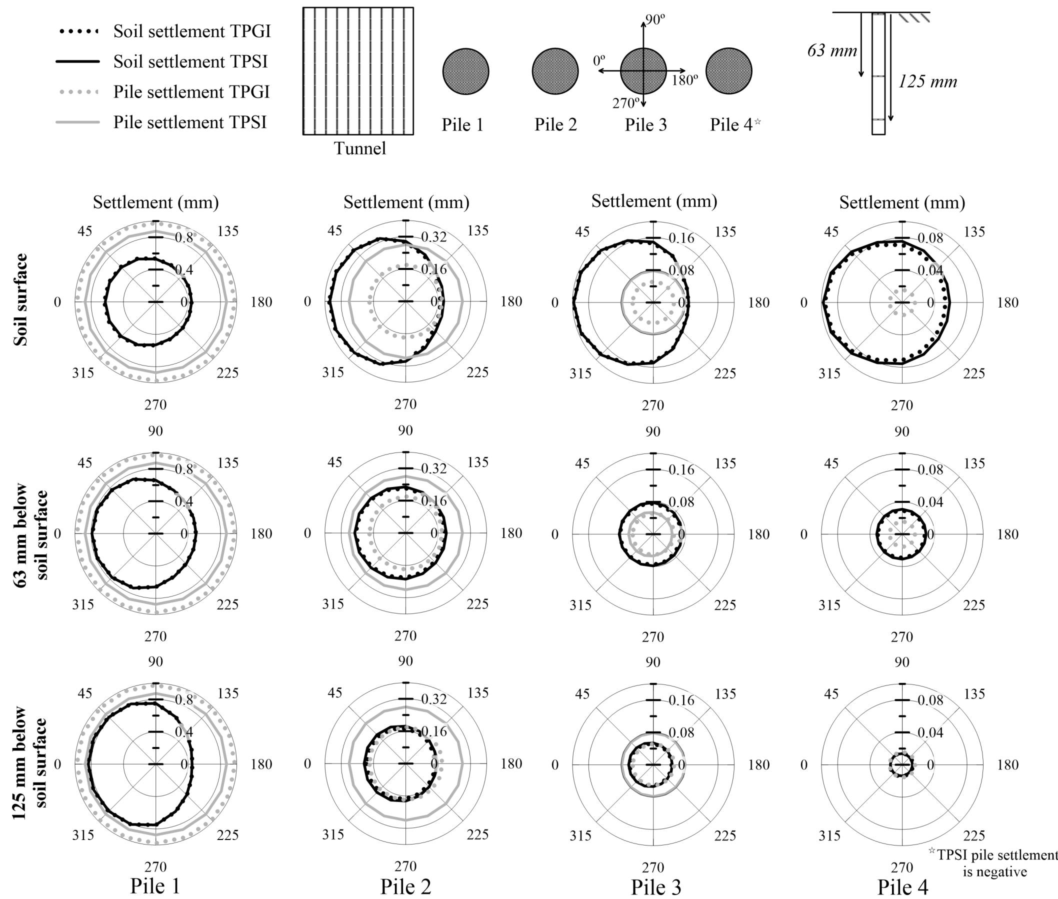

Figure 11: Pile and soil settlement at a tunnel volume loss of $V_{l,t} = 3\%$ for TPGI and TPSI FEA tests

is greater than that of the surrounding soil, indicating an increase in shaft friction along the pile with tunnel volume loss. Referring back to Figure 10, for pile 1 in both centrifuge and FEA tests, the decrease in pile end-bearing load was greater than the decrease in pile head load, indicating an overall increase in shaft resistance along the depth of the pile.

In contrast to pile 1, the non-uniformity of soil settlements for piles 2-4 is greatest at the soil surface, with settlements around the pile becoming more uniform at greater depths. Pile 2 settlement in test TPSI is greater than in test TPGI because of the increase in pile head load (due to mechanism S; as discussed in the previous subsection, the decreased pile 1 head load was transferred to the adjacent piles 2 and 3, see Figure 10). Note that the increase in pile head load for pile 2 in test TPSI was more significant than the increase in pile end-bearing load; see Figure 10(b). To balance the added pile head load, additional pile settlement is required to mobilise resistance; for test TPSI, the tunnelling induced soil settlement was less than pile 2 settlement in the middle and lower portions of the pile, resulting in a mobilisation of increased shaft resistance in this region.

For piles 3 and 4, Figure 11 shows that the pile settlement was less than the surrounding soil at all three depths. The differences in soil settlement between TPGI and TPSI tests for all four piles is insignificant. For pile 4 (farthest away from the tunnel), tunnelling induced soil settlement around the pile is minimal (mechanism T) and similar in magnitude for both TPGI and TPSI tests. Nevertheless, due to the effect of structural stiffness (due to mechanism S causing a decrease in pile head load), pile 4 experienced an upwards (negative) displacement at $V_{l,t} = 3\%$ (refer to Figure 8(d)), hence the pile's settlement is not shown in Figure 11. Note that this upwards movement was not observed in the TPSI centrifuge test, though pile 4 settlement was less in the TPSI test than the TPGI test, showing a consistent trend between centrifuge and numerical results.

4.7. Radial stresses around piles

The numerical analysis results also provide detailed information about the soil stress conditions around the piles and how it is affected by tunnel volume loss, which is not available from the centrifuge tests. This information enables a better understanding of how and why pile load distribution changes during tunnelling. Figure 12 shows the radial stress (σ'_r) around the pile circumference before and after tunnel volume loss ($V_{l,t} = 3\%$) for the TPSI and TPGI FEA tests. The radial stress around the pile is plotted at three depths: 8, 70 and 117 mm below the soil surface. As the radial stress around the pile is two dimensional, the average radial stress around the pile at a given depth can be represented by the size of the 'regions' shown in Figure 12 (this aspect will discussed further in the next subsection), whereas a shift of the centre of the region indicates a stress offset in a particular area of the pile circumference.

Prior to tunnel volume loss ($V_{l,t} = 0\%$), the piles were loaded to the designated working load and the radial stress σ'_r is seen to increase with depth. At this stage, the radial stress is generally uniformly distributed around the pile circumference (the exception to this is near the soil surface, where radial stresses are very low and, at the right side of the pile (farthest from the tunnel), tend to zero; the stresses in this area were affected by the spin-up procedure, where the pile was fixed in place, but the soil moved slightly away from the tunnel).

At $V_{l,t} = 3\%$, for pile 1 (located closest to the tunnel), the radial stress at the lower portion of the pile (117 mm below soil surface) shows a slightly smaller stress region compared to $V_{l,t} = 0\%$ in both TPSI and TPGI tests, indicating that the average radial stress decreased slightly with tunnel volume loss. At the middle and upper portions (70 and 8 mm below soil surface) of pile 1, the size of the stress region is largest at $V_{l,t} = 3\%$ in both tests, indicating an increase of average radial stress. The centres of the regions at $V_{l,t} = 3\%$ for the upper portion of pile 1 are shifted to the right (away from the tunnel), indicating a bias of stress on the far-side of the pile, caused by horizontal movements of the soil towards the tunnel. With tunnel volume loss, test TPGI shows a greater increase in average radial stress at the upper portion of pile 1 than in test TPSI. The detailed stress paths (average radial stress versus shaft resistance around piles) will be discussed in the next subsection.

For pile 2 in both TPGI and TPSI tests, Figure 12 shows that the size of the radial stress regions at all depths is not significantly affected by tunnel volume loss (there is a small overall reduction), but the locations of the centres of the regions is affected, indicating a shift in the bias of stress around the pile. At the middle and upper portions of pile 2, after tunnel volume loss, the bias of radial stress moves to the right (far) side of the pile; as for pile 1, this was caused by horizontal soil movements towards the tunnel. The magnitude of the bias change in test TPGI is greater than TPSI. At the lower portion of pile 2, the bias in stress is shifted to the left (closest to the tunnel). As the base of pile 2 is relatively fixed (tunnelling induced ground movements at the base of pile 2 are minimal), this region acts to resist the lateral movement of the pile (which is being driven to the left by the soil pressures at the upper and middle portions of the pile).

The changes in radial stresses around piles 3 and 4 show similar trends as pile 2, with little change to the average radial stress, a bias of stress to the right of the piles in the middle and upper portions, and a bias of stress to the left of the piles at the lower portion.

In terms of comparison between TPGI and TPSI tests, the magnitude of change in radial stress with tunnelling at the lower and middle portions of the piles is not significant. However, at the upper portion of piles, test TPGI shows a greater shift in the bias of radial stress distribution than the piles in test TPSI. This indicates that the structure stiffness (Mechanism S) predominately affects the development of radial stresses only within the upper portions of the piles; this will be further discussed in the following subsection.

4.8. Computed stress paths at the soil-pile interface

As described in the above subsection, the average radial stress along the middle and upper portions of pile 1 increased with tunnel volume loss, whereas for pile 2 there was minimal change. To further understand the shearing mechanism along the piles, Figure 13 shows the average radial stress versus shaft resistance at the middle portion (70 mm below soil surface) of piles 1 and 2 in the TPGI and TPSI FEA tests. The average radial stress ($\sigma'_{r,ave}$) was calculated as the average value of the radial stress around the pile; the shaft resistance (τ_{ave}) was calculated based on the pile axial forces at that depth of the pile.

Results are provided from the entire FEA test process, which includes

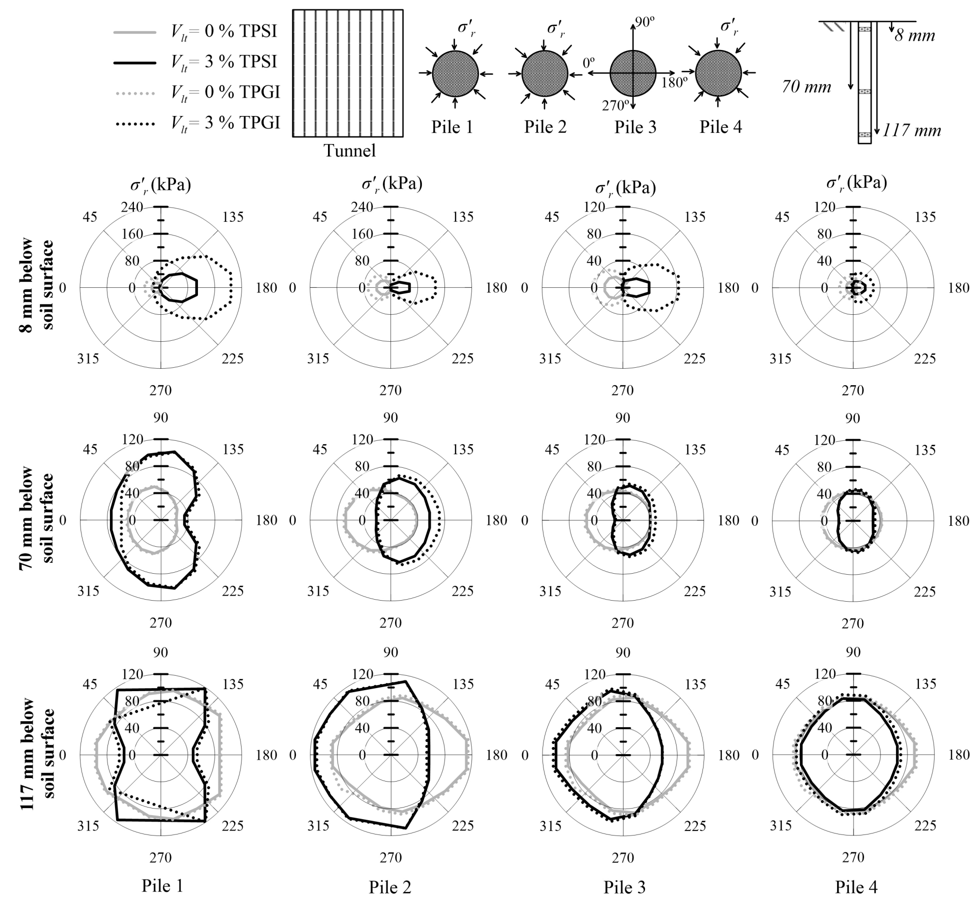

Figure 12: Radial stress around piles before and after tunnel volume loss ($V_{l,t} = 3\%$) for TPGI and TPSI FEA tests

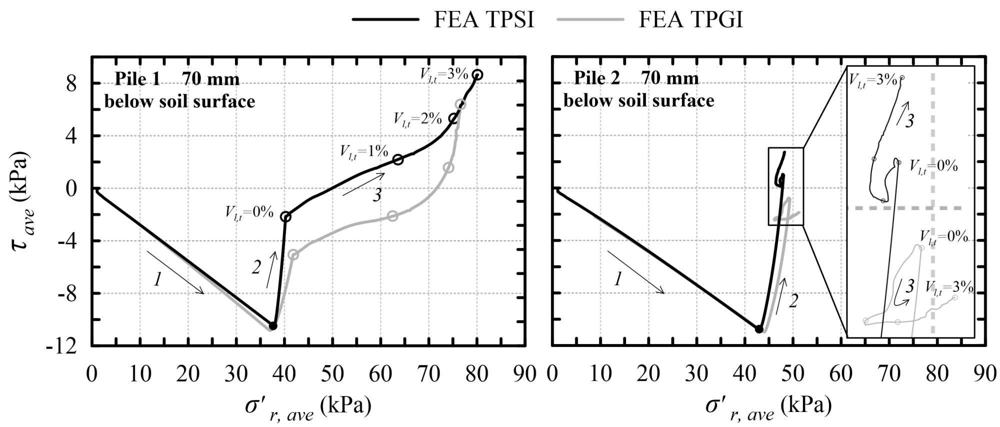

Figure 13: Stress path of the soil elements close to piles 1 and 2 in TPGI and TPSI FEA tests

three stages: (1) spin-up, (2) pile loading, and (3) tunnel volume loss. In stage (1), with the increase in gravity (self-weight of the soil), the average radial stress ($\sigma'_{r,ave}$) at the middle portion of the piles increased. As discussed in Section 5.1, the soil around the piles settled more than the piles and tended to pull the piles downwards, which caused negative shaft resistance along the piles. During spin-up (stage 1), the stress paths between the TPGI and TPSI tests are very similar.

Piles were then loaded to the designated working load (stage 2), during which time the average radial stress around both piles increased; pile 2 shows a greater increase because a higher working load was applied (370 N for pile 2 and 255 N for pile 1). In addition, due to the pile loading, shear resistance increased in both piles. After pile loading, pile 2 shows an increase in shaft resistance, and test TPSI shows positive shaft resistance after pile loading (open circle with $V_{l,t} = 0\%$), whereas shaft resistance in pile 1 remains negative (the applied head load being insufficient to cause the reversal of shaft resistance, as discussed in Section 5.2). Note that the differences between TPSI and TPGI results during pile loading (stage 2), which are most noticeable for pile 1, are due to the influence of structure stiffness in test TPSI (the structure was included in the FEA model at the start of stage 1).

During tunnel volume loss (stage 3), despite that fact that pile 1 head load decreased in test TPSI (due to Mechanism S), both TPGI and TPSI tests show an increase in average radial stress and shaft resistance with tunnelling. Referring back to Figure 11, it was shown that the pile settlement at the middle portion of the pile was greater than the surrounding soil after tunnel volume loss; this relative displacement would cause shearing and potentially dilation of the surrounding soil, which would increase the radial stress and shaft resistance, consistent with the centrifuge results reported by Song and Marshall (2020b). Other mechanisms, such as arching around the tunnel (Franza et al., 2019; Iglesia et al., 2014), would also act to increase radial stresses in this region. For pile 2 in both TPGI and TPSI tests, the stress paths in Figure 13 indicate a complex response to tunnel volume loss. The average radial stress initially shows a decrease with tunnelling (up to $V_{l,t} \approx 1\%$), and then starts to increase, though the magnitude of changes in shaft resistance and average radial stress are relatively small. At the end of tunnel volume loss ($V_{l,t} = 3\%$), pile 2 in test TPSI shows a greater increase in shaft resistance than test TPGI; this occurred because of the increased pile 2 head load in test TPSI due to Mechanism S.

To summarise, the soil-pile interface shearing mechanism during tunnel volume loss is largely affected by the relative distance between the pile and the tunnel. For the pile closest to the tunnel, axial forces along the pile from both centrifuge and numerical tests indicate a decrease in pile end-bearing load with tunnelling, causing the pile to settle relative to the surrounding soil and resulting in increased shaft resistance along the upper and middle portions of the pile. Numerical results from tests TPGI and TPSI suggest that the increase in shaft resistance is less affected by the structure stiffness (Mechanism S). For pile 2 in test TPSI, both centrifuge and numerical tests showed an increase in pile head load due to mechanism S. Based on the axial force distribution along pile 2 (presented in Figure 10), both FEA and centrifuge tests show that most of the increased pile head load was translated to the pile base, indicating that shaft resistance was not significantly affected by tunnelling. For piles further away from the tunnel, the effect of tunnelling on axial force distribution along the piles was insignificant, with little change to shaft resistance.

5. Conclusions

This paper used results from hybrid centrifuge tests and numerical simulations to study the complex interaction between tunnelling induced ground displacements and a piled structure. Two cases are presented in the paper: a tunnel-pile group interaction (TPGI) in which pile head load remains constant, and a tunnel-piled structure interaction (TPSI) where piles were connected (virtually within the hybrid centrifuge test) to a five-storey steel frame. Both cases considered a row of four piles running transverse to the tunnel direction, with pile tips located just above the depth of the tunnel crown, and with the nearest pile located to the side of the tunnel. An advanced hypoplastic constitutive model was used for numerical simulations of the centrifuge tests, providing results that were consistent with the mechanisms observed from centrifuge test results. The numerical simulations enabled an in-depth analysis of the response of piles to tunnelling and the role that a connected structure plays (i.e. contrasting the TPGI and TPSI cases). The following conclusions can be made from the work:

- During spin-up, both numerical and centrifuge tests showed an increase in axial force along the piles; at the upper portion of the piles, the soil settled more than the piles, with negative shaft friction developing and pulling the piles downwards. The magnitude of the negative shaft resistance in the numerical simulations was much smaller than the centrifuge tests.

- During pile loading, numerical simulations showed that the majority of added pile head load was taken by the pile end-bearing load, whereas centrifuge results indicated that most of the increased pile head load was taken by the shaft resistance.

- The discrepancies between numerical and centrifuge results during spin-up and pile loading were related to the accuracy of the adopted FEA interface element and the difference in radial stresses developing around the piles; it was shown that the lateral stresses acting on the piles in the centrifuge were likely considerably larger than within the FEA simulations, which is due to the limitation of the adopted FEA soil-pile interface model (Coulomb friction law).

- Pile settlements in the numerical simulations were greater than those measured in the centrifuge tests in general, however the numerical results provided a good prediction of the difference in pile settlement between the TPGI and TPSI tests. For the TPSI case, the numerical simulation over-predicted the change in pile head load.

- Results demonstrated the effect of two important mechanisms affecting pile head load, the axial force distribution along piles, and pile settlement: Mechanism T related to tunnelling induced ground displacements, and Mechanism S related to the structure stiffness. Mechanism T is typically considered within tunnel design risk assessments, whereas Mechanism S, which was shown to have a significant effect on pile head loads, is generally disregarded.

- The amount of load redistribution due to structural stiffness (Mechanism S) in the centrifuge and numerical models agreed well. The head load of the pile closest to the tunnel reduced by about 20% at a tunnel volume loss of 3%, whereas the head load of the adjacent pile increased by about 18% (the building considered in this study was relatively flexible in shear; more rigid buildings will have a greater effect on pile head load redistribution). This level of load redistribution may be important when considering foundations with low safety factors (for pile loading) or where piles are susceptible to damage from tensile stresses (Franza et al., 2021a,b).

- Numerical simulations showed that the soil settlement around the pile circumference was not uniform with tunnelling; the near-side (relative to the tunnel) soil settles more than the far-side. In addition, both centrifuge and numerical tests showed that Mechanism S had an effect on soil and pile settlements, consequently affecting the shaft resistance development (though centrifuge test results indicated that the effect of Mechanism S on pile displacements may not be significant for practical considerations; more study including a wider parametric study is needed here).

- Numerical results were used to demonstrate how tunnelling affects the radial stress profile around piles. The changes to radial stresses around the piles were dominated by the effect of tunnelling induced ground displacements, causing a general pattern of increased stresses on the far-side of the piles along the middle to upper portions of the piles, caused by the movement of soil in this region. This was accompanied by an increase in radial stresses on the near-sides of the piles along the bottom portion as a way of achieving horizontal equilibrium. The exception to this was the pile closest the tunnel, where, near the pile tip, a general reduction of radial stress was observed due to the stress relaxation caused by tunnelling.

- The computed stress paths at the soil-pile interface from the numerical simulations suggested that, for the pile located closest to the tunnel, with pile settlement, shaft resistance and average radial stress increase with tunnelling along the middle and upper portions of the pile. The stress paths along other piles (further away from the tunnel), though complex, showed relatively small changes in radial stress and shaft resistance.

The current study focused on evaluating the consequence of tunnel excavation on an adjacent piled structure in sand. Future research is needed to better understand the effect of soil, foundation, building, and geometric parameters, in addition to consideration of how protective measures could be incorporated, such as the use of protective walls between the tunnel and foundation.

823 # 6. NOTATION

B_{bay}	The spacing of bay
C	Depth of cover above the tunnel
C_u	Coefficient of uniformity
d_e	Distance between the pile and tunnel (Pile 1)
d_p	Diameter of the pile
D_t	Diameter of the tunnel (d_t)
D_{50}	Average size of the soil particle
e_{max}	Maximum void ratio
e_{min}	Minimum void ratio
e_{c0}	Critical void ratio at zero pressure
e_{d0}	Minimum void ratio at zero pressure
e_{i0}	Maximum void ratio at zero pressure
824 e_{p0}	Initial void ratio of compression test at zero pressure
e_{max}	Maximum void ratio
E	Young's modulus
EA	Axial stiffness
EI	Flexural rigidity
G_s	Specific gravity
H_{storey}	Height of the building storey in prototype scale
h_s	Granular hardness
I_d	Relative density
K_0	Static earth pressure coefficient
L_p	Pile length, measured from ground surface to pile tip
n	Controls curve fitting parameter
S_p	Pile settlement

S_t	Spacing between piles
S_v	Soil settlement; vertical displacement
$V_{l,t}$	Tunnel volume loss, in %
α	Governs the peak friction angle of the soil
β	Governs the soil stiffness
σ'_v	Vertical effective stress
σ'_r	Radial effective stress
$\sigma'_{r,ave}$	average radial effective stress
τ_{av}	Average shaft resistance
ϕ'_c	Critical state friction angle
ν	Poisson's ratio

7. Supplemental data

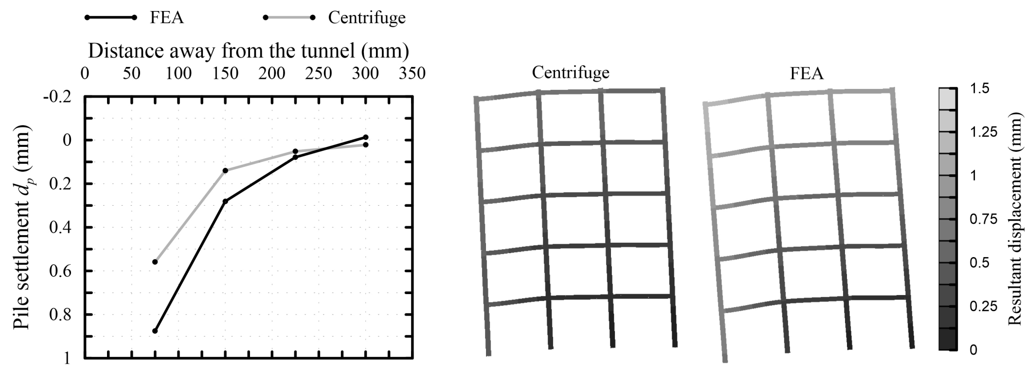

Figure S1: Deformed shape at a tunnel volume loss of $V_{l,t} = 3\%$ for test TPSI

References

Addenbrooke, T., Potts, D., Puzrin, A., 1997. The influence of pre-failure soil stiffness on the numerical analysis of tunnel construction. Géotechnique 47, 693–712.

Boonsiri, I., Takemura, J., 2015. Observation of ground movement with existing pile groups due to tunneling in sand using centrifuge modelling. Geotechnical and Geological Engineering 33, 621–640.

Cheng, C.Y., Dasari, G.R., Chow, Y.K., Leung, C.F., 2007. Finite element analysis of tunnel–soil–pile interaction using displacement controlled model. Tunnelling and Underground Space Technology 22, 450–466.

Devriendt, M., Williamson, M., 2011. Validation of methods for assessing tunnelling-induced settlements on piles. Ground Eng , 25–30.

Franza, A., Marshall, A.M., 2019. Centrifuge and real-time hybrid testing of tunnelling beneath piles and piled buildings. ASCE Journal of Geotechnical and Geoenvironmental Engineering 145, 04018110. doi:10.1061/(ASCE)GT.1943-5606.0002003.

Franza, A., Marshall, A.M., Jimenez, R., 2021a. Nonlinear soil-pile interaction induced by ground settlements: pile displacements and internal forces. Géotechnique 71, 239–248.

Franza, A., Marshall, A.M., Zhou, B., 2019. Greenfield tunnelling in sands: the effects of soil density and relative depth. Geotechnique 69, 297–307. doi:10.1680/jgeot.17.p.091.

Franza, A., Zheng, C., Marshall, A.M., Jimenez, R., 2021b. Investigation of soil-pile-structure interaction induced by vertical loads and tunnelling. Computers and Geotechnics In press. doi:10.1016/j.compgeo.2021.104386.

Gulvanessian, H., Formichi, P., Calgaro, J.A., 2009. Designers' Guide to Eurocode 1: Actions on Buildings: EN1991-1-1 and-1-3 TO-1-7. Thomas Telford Ltd.

Herle, I., Gudehus, G., 1999. Determination of parameters of a hypoplastic constitutive model from properties of grain assemblies. Mechanics of Cohesive-frictional Materials 4, 461–486.

Hibbitt, K., 2002. ABAQUS/Explicit User's Manual: Version 6.3. Hibbit, Karlsonn & Sorensen.

Hong, Y., Soomro, M.A., Ng, C., 2015. Settlement and load transfer mechanism of pile group due to side-by-side twin tunnelling. Computers and Geotechnics 64, 105–119.

Idinyang, S., Franza, A., Heron, C., Marshall, A.M., 2018a. Real-time data coupling for hybrid testing in a geotechnical centrifuge. International Journal of Physical Modelling in Geotechnics doi:doi.org/10.1680/jphmg.17.00063.

Idinyang, S., Franza, A., Heron, C., Marshall, A.M., 2018b. Real-time data coupling for hybrid testing in a geotechnical centrifuge. International Journal of Physical Modelling in Geotechnics , 1–13.

Iglesia, G.R., Einstein, H.H., Whitman, R.V., 2014. Investigation of Soil Arching with Centrifuge Tests. Journal of Geotechnical and Geoenvironmental Engineering 140, 04013005. doi:10.1061/(asce)gt.1943-5606.0000998.

Jacobsz, S.W., 2003. The effects of tunnelling on piled foundations. Ph.D. thesis. University of Cambridge.

Jacobsz, S.W., Standing, J.R., Mair, R.J., Hagiwara, T., Sugiyama, T., 2004. Centrifuge modelling of tunnelling near driven piles. Soils and Foundations 44, 49–56.

Jardine, R.J., Symes, M.J., Burland, J.B., 1984. The measurement of soil stiffness in the triaxial apparatus. Géotechnique 34, 323–340. doi:10.1680/geot.1984.34.3.323.

Kaalberg, F.J., Teunissen, E.A.H., Van Tol, A.F., Bosch, J.W., 2005. Dutch research on the impact of shield tunnelling on pile foundations, in: Klaas Jan Bakker, Adam Bezuijen, W.B.E.K. (Ed.), Proceedings of the 5th International Symposium on Geotechnical Aspects of Underground Construction in Soft Ground, Taylor & Francis Group. pp. 123–131.

Lee, C.J., Chiang, K.H., 2007. Responses of single piles to tunneling-induced soil movements in sandy ground. Canadian Geotechnical Journal 44, 1224–1241. URL: https://doi.org/10.1139/T07-050, arXiv:https://doi.org/10.1139/T07-050.

Li, Y., Zhang, W., 2020. Investigation on passive pile responses subject to adjacent tunnelling in anisotropic clay. Computers and Geotechnics 127. doi:10.1016/j.compgeo.2020.103782.

Loganathan, N., Poulos, H.G., Stewart, D.P., 2000. Centrifuge model testing of tunnelling-induced ground and pile deformations. Geotechnique 50, 283–294.

Mair, R.J., Taylor, R.N., Burland, J.B., 1996. Prediction of ground movements and assessment of risk of building damage due to bored tunnelling, in: Mair, R.J., Taylor, R.N. (Eds.), Geotechnical Aspects of Underground Construction in soft ground, Balkema, London. pp. 713–718.

Marshall, A.M., Mair, R.J., 2011. Tunneling beneath driven or jacked end-bearing piles in sand. Canadian Geotechnical Journal 48, 1757–1771.

Ng, C.W.W., Hong, Y., Soomro, M., 2015. Effects of piggyback twin tunnelling on a pile group: 3d centrifuge tests and numerical modelling. Géotechnique 65, 38–51.

Ng, C.W.W., Lu, H., Peng, S.Y., 2013. Three-dimensional centrifuge modelling of the effects of twin tunnelling on an existing pile. Tunnelling and Underground Space Technology 35, 189–199.

Ng, C.W.W., Soomro, M.A., Hong, Y., 2014. Three-dimensional centrifuge modelling of pile group responses to side-by-side twin tunnelling. Tunnelling and underground space technology 43, 350–361.

Schoor, J., R, W., Yin, K., Stephenson, V., 2021. Assessing the impacts of construction-induced ground movement on framed buildings, C796. Technical Report. CIRIA. London, UK.

Selemetas, D., 2005. The response of full-scale piles and piled structures to tunnelling. Ph.D. thesis. University of Cambridge.

Selemetas, D., Standing, J.R., 2017. Response of full-scale piles to EPBM tunnelling in London Clay. Geotechnique .

Song, G., Marshall, A.M., 2020a. Centrifuge modelling of tunnelling induced ground displacements : pressure and displacement control tunnels. Tunnelling and Underground Space Technology 103, 103461. doi:10.1016/j.tust.2020.103461.

Song, G., Marshall, A.M., 2020b. A centrifuge study on the influence of tunnel excavation on piles in sand. ASCE Journal of the Geotechnical and Geoenvironmental Engineering 146, 04020129.

Song, G., Marshall, A.M., Heron, C., 2018. A mechanical displacement control model tunnel for simulating eccentric ground loss in the centrifuge, in: 9th International Conference of Physical Modelling in Geotechnics: ICPMG.

Song, G., Xu, J., Heron, C.M., Marshall, A.M., Correia, R., Korposh, S., 2021. The application of FBGs for centrifuge testing: pile axial loads and wall bending moments. International Journal of Physical Modelling in Geotechnics In press, 1–33. URL: https://doi.org/10.1680/jphmg.20.00078, doi:10.1680/jphmg.20.00078.

Soomro, M.A., Ng, C.W.W., Memon, N., Bhanbhro, R., 2018. Lateral behaviour of a pile group due to side-by-side twin tunnelling in dry sand:

3d centrifuge tests and numerical modelling. Computers and Geotechnics 101, 48–64.

Stutz, H., Mašín, D., Wuttke, F., 2016. Enhancement of a hypoplastic model for granular soil–structure interface behaviour. Acta Geotechnica 11, 1249–1261.

Wang, H., Leung, C.F., Yu, J., Huang, M., 2020. Axial response of short pile due to tunnelling-induced soil movement in soft clay. International Journal of Physical Modelling in Geotechnics 20, 71–82. URL: https://doi.org/10.1680/jphmg.18.00045, doi:10.1680/jphmg.18.00045.

Williamson, M.G., Mair, R.J., Devriendt, M.D., Elshafie, M.Z.E.B., 2017a. Open-face tunnelling effects on non-displacement piles in clay – part 1 : centrifuge modelling techniques. Géotechnique 67, 983–1000. doi:10.1680/jgeot.SIP17.P.120.

Williamson, M.G., Mair, R.J., Devriendt, M.D., Elshafie, M.Z.E.B., 2017b. Open-face tunnelling effects on non-displacement piles in clay – part 2 : tunnelling beneath loaded piles and analytical modelling. Géotechnique 67, 1001–1019. doi:10.1680/jgeot.SIP17.P.120.

von Wolffersdorff, P.A., 1996. A hypoplastic relation for granular materials with a predefined limit state surface. Mechanics of Cohesive-frictional Materials 1, 251–271.

Xu, J., Franza, A., Marshall, A.M., 2020. Response of framed buildings on raft foundations to tunneling. Journal of Geotechnical and Geoenvironmental Engineering 146, 04020120. doi:10.1061/(ASCE)GT.1943-5606.0002376.